ARTICLE

Check for updates

Symmetry-protected Bose-Einstein condensation of interacting hardcore bosons

Reja H. Wilke [1,2✉], Thomas Köhler [3], Felix A. Palm [1,2] & Sebastian Paeckel [1,2]

The large practical potential of exotic quantum states is often precluded by their notorious fragility against external perturbations or temperature. Here, we introduce a mechanism stabilizing a one-dimensional quantum many-body phase exploiting an emergent $\mathbb{Z}_2$-symmetry based on a simple geometrical modification, i.e. a site that couples to all lattice sites. We illustrate this mechanism by constructing the solution of the full quantum many-body problem of hardcore bosons on a wheel geometry, which are known to form Bose-Einstein condensates. The robustness of the condensate against interactions is shown numerically by adding nearest-neighbor interactions, which typically destroy Bose-Einstein condensates. We discuss further applications such as geometrically inducing finite-momentum condensates. Since our solution strategy is based on a generic mapping, our findings are applicable in a broader context, in which a particular state should be protected, by introducing an additional center site.

[1] Department of Physics, Arnold Sommerfeld Center for Theoretical Physics (ASC), Ludwig-Maximilians-Universität München, 80333 München, Germany. [2] Munich Center for Quantum Science and Technology (MCQST), Schellingstr. 4, D-80799 München, Germany. [3] Department of Physics and Astronomy, Uppsala University, Box 516, S-751 20 Uppsala, Sweden. ✉email: reja.wilke@physik.uni-muenchen.de

The ability to control and manipulate quantum systems has seen a remarkable development in the past two decades. For instance, cold atom experiments have become a versatile platform to realize various exotic quantum phases of matter[1–8]. Available experimental setups nowadays allow for the control of both geometry and interactions of simulated model systems. It is thus crucial to theoretically identify physical mechanisms that improve the stability and scaling properties of exotic quantum phases, which then might be realized and tested in experiments. In that context, remarkable progress in understanding the stability of Bose-Einstein condensates (BEC) has been made by analyzing spectral properties of a wheel of hardcore bosons (HCB)[9–12] as depicted in Fig. 1a. This model features an energy scale $\sim \sqrt{L}$ that is generated by the extensively scaling coordination number of a center site, which in this geometry is given by the number of ring sites L. While large coordination numbers appeared in several theoretical approaches[13–18], the underlying mechanism as well as its stability against perturbations remained an open question.

Here we show that the observed stability of the BEC phase on the wheel lattice is no physical oddity, but a consequence of the geometry of the wheel lattice itself, hosting a hidden $\mathbb{Z}_2$-symmetry. For that purpose, we present a mapping that allows us to construct the solution of a family of quantum many-body problems with arbitrary k_0-modulated ring-to-center hoppings $s_j = se^{ik_0 j}$, and to analyze the formation of a BEC phase with momentum k_0. In the context of central spin models[19–24] a solution strategy to a similar problem is based on the Bethe ansatz and has been applied to describe for instance Rydberg impurities in ultracold atomic quantum gases[25]. In contrast, we derive an analytical expression by introducing a mapping to a ladder system of spinless fermions (SF) which becomes exact both in the thermodynamic limit and at low densities. We emphasize that this mapping can be applied in various other setups to analytically tackle problems with an extensively scaling coordination number. In the context of hardcore bosons, our approach reveals that the stabilizing mechanism for the BEC is the extensively scaling coordination number of the center site, introducing a robust

discrete $\mathbb{Z}_2$-symmetry that protects the ordered quantum many-body phase against local perturbations on the outer ring. Furthermore, we trace back the protection to odd-parity $k = k_0$ single-particle states that are gapped out $\sim s\sqrt{L} \equiv \tilde{s}$. This property implies that in the thermodynamic limit the system immediately transitions into a BEC, as long as there is a finite ring-to-center hopping rate $s > 0$, which remarkably also holds when adding local interactions to the outer ring. We demonstrate, beyond previous work, the robust protection of the BEC numerically, using density-matrix renormalization group (DMRG)[26–29] simulations to calculate the k_0-condensate fraction when adding nearest-neighbor interactions, for a wide parameter range and various particle number densities. As a consequence, the $\mathbb{Z}_2$-symmetry in principle allows to experimentally tune the transition temperature of a gas of interacting HCB by modifying the wheel's coordination number. Here, we show that the central quantity is the ratio $\frac{V}{s}$ between the interaction strength V and the renormalized ring-to-center hopping, as we demonstrate by further numerical results. Finally, our analysis implies that the emergent $\mathbb{Z}_2$-symmetry is generically induced by the model's geometry. Therefore, general k_0-modulated hoppings give rise to corresponding protected k_0 modes and the respective single-particle states are gapped out $\sim s\sqrt{L}$. This paves the way to a generic mechanism that can be exploited in various contexts, for instance, to stabilize exotic quantum many-body phases such as $k_0 \neq 0$, i.e. finite momentum BEC[30–33].

Results
In order to demonstrate our mapping and its implications, we consider HCB on a L-sited ring with an additional center site[10,12] (see Fig. 1a). The model exhibits k_0-modulated ring-to-center hopping $s_j = se^{ik_0 j}$ while the homogeneous hopping on the ring is tuned by a parameter t. The corresponding Hamiltonian reads

$$\hat{H} \equiv -t \sum_{j=0}^{L-1} \left(\hat{h}_j^\dagger \hat{h}_{j+1} + \text{h.c.} \right) - \sum_{j=0}^{L-1} \left(s_j \hat{h}_j^\dagger \hat{h}_\odot + \text{h.c.} \right), \quad (1)$$

where $\hat{h}_j^{(\dagger)}$ is the HCB ladder operator on the j-th site of the ring and $\hat{h}_\odot^{(\dagger)}$ on the center site, spanning the overall Hilbert space $\mathcal{H}_2^{\otimes L+1}$. In the limit $\frac{s}{t} \to 0$ (ring geometry) the model exhibits off-diagonal quasi long-range order, indicated by the algebraic decay of the single-particle density matrix (SPDM) $\rho_{ij} \sim |x_i - x_j|^{-\frac{1}{2}}$[34,35]. This leads to the formation of a quasi-BEC, i.e. the ground state is a bosonic condensate whose occupation scales as $\sqrt{N}$[36,37], where N denotes the number of HCB.

The opposite limit, $\frac{s}{t} \to \infty$ (star geometry), has been shown recently to feature a real BEC where the occupation in the ground state scales as $L\rho(1 - \rho + 1/L)$ with $\rho = N/L$[11].

Analytical solution via wheel-to-ladder mapping. The property of Eq. (1) to interpolate between two superficially disconnected physical situations, one exhibiting no stable long-range order ($\frac{s}{t} = 0$) and one featuring true long-range order ($\frac{s}{t} \to \infty$), calls for a deeper understanding of the underlying physics. For that purpose, we demonstrate how to construct an analytical solution of Eq. (1) and, thereby, learn about the origin of the emergence of true long-range order. From a theoretical point of view, finding the eigenstates is hindered by the fact that under a Fourier transformation, HCB loose their hardcore property. Typically, this is accounted for by mapping the HCB to spinless fermions via a Jordan-Wigner transformation (JWT) which, however, requires to introduce a normal ordering, for instance via a chain mapping. Here, the additional center site complicates the situation, since it couples to any other lattice site in the chain mapping, generating arbitrarily long-ranged interactions. We
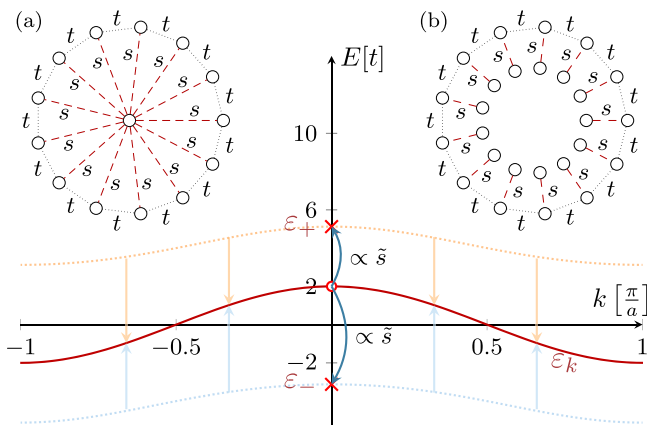

Fig. 1 Wheel geometry, ladder geometry and the single-particle dispersion. The main plot illustrates the single-particle dispersion relation (middle, red curve) of the wheel geometry (**a**), emerging from projecting down the dispersion from the ladder geometry (**b**) (upper orange and lower blue curve). Note the appearance of two single-particle states at $k_0 = 0$ (red crosses). This is because the Hilbert space of the wheel is obtained by projecting out all modes on the inner ring, except for the zero momentum states $|N_{\odot,k=0}\rangle_\odot$. Momentum conservation then couples this central mode to the particular mode on the outer ring respecting the k_0-modulated ring-to-center hopping, which generates an extensively scaling level splitting (red circle and crosses).
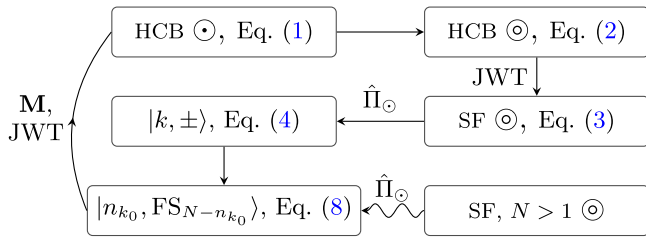
Fig. 2 Solution strategy for Eq. (1). The hardcore boson (HCB) wheel $\odot$ is transformed to a ladder $\circleddot$, which is then mapped to a ladder of spinless fermions (SF) via a Jordan-Wigner transform (JWT). From the ladder of SF, the single-particle spectrum $|k, \pm\rangle$ and therefrom projected Slater determinants $\big|n_{k_0}, \mathrm{FS}_{N-n_{k_0}} big\rangle$ are constructed, utilizing the projector to the $N_\odot \leq 1$ subspace, $\hat{\Pi}_\odot$. The constructed many-particle Slater determinants finally allow for the analytic solution of the HCB wheel diagonalizing a 4×4 matrix **M**. Note that no closed solution of the SF ladder Hamiltonian is required (only its projected counterpart).

introduce a mapping from the wheel Eq. (1) to a ladder geometry of HCB with periodic boundary conditions (see Fig. 1b) to resolve this issue. Physically, the coupling to an inner ring allows to disentangle the complications arising from arbitrary long-ranged hoppings of particles on the outer ring that are generated by second order processes. The overall solution strategy is sketched schematically in Fig. 2. The crucial step is to identify the central Hilbert space of the HCB wheel with the subspace of the single-particle momentum states $\big|N_{\odot,k=0}\big\rangle_\odot$ on the inner ring of the ladder (enforcing occupations $N_{\odot,k=0} \equiv N_\odot \leq 1$). The projector $\hat{\Pi}_\odot$ to this subspace allows us to construct a solution on the expanded Hilbert space of the ladder geometry and eventually project down. In Supplementary Note 3, we observe that the JWT of the projector becomes asymptotically diagonal in both the thermodynamic limit and at low densities. Therefore, the long-range coupled wheel Hamiltonian can be mapped to an only next-nearest-neighbor (NNN) coupled ladder Hamiltonian $\hat{H}_{\mathrm{lad}}$:

$$\hat{H} = \hat{\Pi}_\odot \hat{H}_{\mathrm{lad}} \hat{\Pi}_\odot. \tag{2}$$

While the full details of the mapping can be found in Supplementary Note 1, the most important observation is that a JWT of $\hat{H}_{\mathrm{lad}}$ introduces only local parity operators $e^{i\pi\hat{n}_{\odot,j}}$:

$$\hat{\Pi}_\odot \hat{H}_{\mathrm{lad}} \hat{\Pi}_\odot = t \sum_j \hat{\Pi}_\odot \left(\hat{c}_j^\dagger e^{i\pi\hat{n}_{\odot,j}} \hat{c}_{j+1} + \mathrm{h.c.} \right) \hat{\Pi}_\odot \\ - \tilde{s} \sum_j \hat{\Pi}_\odot \left(e^{ik_0 j} \hat{c}_j^\dagger \hat{c}_{\odot,j} + \mathrm{h.c.} \right) \hat{\Pi}_\odot, \tag{3}$$

wherein $\hat{c}_j^{(\dagger)}$ ($\hat{c}_{\odot,j}^{(\dagger)}$) denotes the fermionic ladder operator on the j-th site of the outer (inner) ring and the single-site number operator on the inner ring is given by $\hat{n}_{\odot,j} = \hat{c}_{\odot,j}^\dagger \hat{c}_{\odot,j}$. We emphasize the appearance of a rescaled ring-to-center hopping amplitude $\tilde{s} = s\sqrt{L}$, which allows to connect to the known solutions when taking the thermodynamic limit $L \to \infty$. In fact, in the thermodynamic limit, the wheel immediately collapses to the star geometry whenever there is a fixed, finite ratio $\frac{s}{t}$, and the ground state is a true BEC. However, the question remains what happens for fixed ratios $\frac{\tilde{s}}{t}$. This matters for finite system sizes, as for example in mesoscopic systems, and ultracold atomic gas experiments, in particular Rydberg atoms. In particular, we are interested in the impact of the extensive energy scale set by $\tilde{s}$ on the formation and stability of the BEC, which requires a more in-depth analysis of the ground state of Eq. (3). Note that for now and in the following, we refer to the scaling of the ring-to-center hopping $\tilde{s} = s\sqrt{L}$ as extensive in the system size.

As we show in Supplementary Note 2, it is instructive to first solve Eq. (3) for the single-particle eigenstates $|k, \pm\rangle$, fulfilling $\langle e^{i\pi\hat{n}_{\odot,j}} \rangle \equiv 1$:

$$|k, \pm\rangle = \begin{cases} \hat{c}_k^\dagger |\varnothing\rangle & \text{if } k \neq k_0, \\ \psi_\pm \left(\hat{c}_k^\dagger + \Delta_\pm \hat{c}_{\odot,k=0}^\dagger \right) |\varnothing\rangle & \text{if } k = k_0. \end{cases} \tag{4}$$

Here, $\hat{c}_{(\odot),k}^\dagger = \frac{1}{\sqrt{L}} \sum_{j=0}^{L-1} e^{-ikj} \hat{c}_{(\odot),j}^\dagger$ with $\psi_{(k),\pm}$ being a normalization constant and $|\varnothing\rangle$ denotes the vacuum state. As shown in Fig. 1, the corresponding single-particle spectrum is identical to that of a tight-binding chain (i.e., $\varepsilon_k = 2t \cos k$) except for the $k = k_0$ states whose single-particle energies are characterized by the splitting $\Delta_\pm = \frac{\varepsilon_0}{2\tilde{s}} \pm \frac{\sqrt{\varepsilon_0^2 + 4\tilde{s}^2}}{|2\tilde{s}|}$:

$$\varepsilon_\pm = \frac{1}{2} \left(\varepsilon_0 \pm \mathrm{sgn}(\tilde{s}) \sqrt{\varepsilon_0^2 + 4\tilde{s}^2} \right) = \tilde{s}\Delta_\pm. \tag{5}$$

These $k = k_0$ single-particle eigenstates Eq. (4) separate $\propto |\tilde{s}| \propto \sqrt{L}$ from the remaining spectrum giving rise to a single-particle gap. Referring to Eq. (3), in the limit $\frac{\tilde{s}}{t} \to \infty$, the hopping on the outer ring can be neglected, and the same holds for the impact of the JWT on the overall eigenstate. Consequently, the single-particle gap can be expected to control the many-body spectrum, in this limit. Additionally, from $\Delta_\pm \xrightarrow{\tilde{s}/t \to \infty} \pm 1$ we find that the corresponding wavefunction is characterized by maximally mixing the distinguished mode $|k_0\rangle$ on the outer ring with the state $\big|N_\odot = 1\big\rangle_\odot$ on the inner ring. This highly non-local wavefunction, generated from the extensive scaling of Eq. (5), already suggests the stability of the BEC under local perturbations on the outer ring.

In order to further elaborate on the extensive scaling property, we now return to the solution of Eq. (1) with the complete derivation detailed in the Supplementary Note 4. Here, the key observation is that Slater determinants $\big|\mathrm{FS}_N\big\rangle = |k_1, \ldots, k_N\rangle$ constructed from a set of N single-particle states Eq. (4) with $k \neq k_0$ are also eigenstates of $\hat{H} = \hat{\Pi}_\odot \hat{H}_{\mathrm{lad}} \hat{\Pi}_\odot$:

$$\hat{\Pi}_\odot \hat{H}_{\mathrm{lad}} \hat{\Pi}_\odot \big|\mathrm{FS}_N\big\rangle = \left(\sum_{l=1}^N \varepsilon_{k_l} \right) \hat{\Pi}_\odot \big|\mathrm{FS}_N\big\rangle. \tag{6}$$

This observation can be understood by noting that the projected parity operator in Eq. (3) can be written in terms of the zero momentum density $N_\odot$ on the inner ring

$$\hat{\Pi}_\odot e^{i\pi\hat{n}_{\odot,j}} \hat{\Pi}_\odot = \hat{1}_{\odot,j} - \frac{2}{L} \hat{c}_{\odot,k=0}^\dagger \hat{c}_{\odot,k=0}, \tag{7}$$

and thus $\hat{\Pi}_\odot e^{i\pi\hat{n}_{\odot,j}} \hat{\Pi}_\odot \big|\mathrm{FS}_N\big\rangle = \big|\mathrm{FS}_N\big\rangle$. Particle-number conservation of the wheel Hamiltonian then motivates to construct an ansatz for the N-particle eigenstates, superimposing all possible occupations of the k_0 mode that belong to the same overall particle number sector

$$|\psi_N\rangle = \alpha_0 \big|\mathrm{FS}_N\big\rangle + \left(\alpha_{1_+} \hat{\psi}_+^\dagger + \alpha_{1_-} \hat{\psi}_-^\dagger \right) \big|\mathrm{FS}_{N-1}\big\rangle \\ + \alpha_2 \hat{\psi}_+^\dagger \hat{\psi}_-^\dagger \big|\mathrm{FS}_{N-2}\big\rangle, \tag{8}$$

with complex coefficients $\alpha_{0,1_\pm,2}$. These states describe a superposition of either empty ($\propto \alpha_0$) or doubly occupied ($\propto \alpha_2$) k_0 states and highly non-local states $\propto \alpha_{1_\pm}$ in which the k_0 mode on the outer ring is coupled to the $\big|N_\odot = 1\big\rangle_\odot$ mode on the inner ring.

Using the orthogonality of different Slater determinants, it is a straightforward calculation to find that the general solution of the eigenvalue problem $\hat{\Pi}_\odot \hat{H}_{\mathrm{lad}} \hat{\Pi}_\odot \big|\mathrm{FS}_N\big\rangle = E \hat{\Pi}_\odot \big|\mathrm{FS}_N\big\rangle$ is reduced to the diagonalization of a 4×4 matrix. Fixing a Slater determinant

$|\text{FS}_N\rangle$ and two modes $k', k'' \neq k_0$ so that $\hat{c}_{k'}|\text{FS}_N\rangle = |\text{FS}_{N-1}\rangle$ as well as $\hat{c}_{k''}\hat{c}_{k'}|\text{FS}_N\rangle = |\text{FS}_{N-2}\rangle$, and labeling the 4 basis states by their possible occupations of the $k = k_0$ mode $n_{k_0} = 0, 1_\pm, 2$, the resulting eigenvalue problem is of the form

$$
\begin{pmatrix} h_0 & & \\ & \boxed{h_1} & \\ & & h_2 \end{pmatrix} \begin{pmatrix} \alpha_0 \\ \alpha_{1_+} \\ \alpha_{1_-} \\ \alpha_2 \end{pmatrix} = E \begin{pmatrix} \alpha_0 \\ \alpha_{1_+} \\ \alpha_{1_-} \\ \alpha_2 \end{pmatrix} \quad (9)
$$

with $h_0 = \langle 0|\hat{H}_{\text{lad}}|0\rangle$, $h_1 = \langle 1_\mu|\hat{H}_{\text{lad}}|1_{\mu'}\rangle$ for $\mu, \mu' \in \{+, -\}$, and $h_2 = \langle 2|\hat{H}_{\text{lad}}|2\rangle$. Note the block-diagonal structure that reflects the different $k = k_0$ parities, i.e.

$$
e^{i\pi\hat{n}_{k_0}}|n_{k_0}\rangle = \begin{cases} |n_{k_0}\rangle, & \text{if } n_{k_0} = 0, 2, \\ -|n_{k_0}\rangle, & \text{if } n_{k_0} = 1_+, 1_-. \end{cases} \quad (10)
$$

We emphasize the existence of a hidden $\mathbb{Z}_2$-symmetry of the many-body eigenstates. This symmetry is an immediate consequence of the modulation of the hopping to the center site, i.e. it characterizes the k_0-occupation. Furthermore, condensation requires a breaking of particle number conservation on the outer ring, which is possible only in the $n_{k_0} = 1_\pm$ subspace. Thus, an odd $\mathbb{Z}_2$-symmetry of the ground state signals the formation of a BEC.

Upon solving Eq. (9), a special structure of the many-body spectrum appears that is characterized by a clustering of eigenstates belonging to the same k_0-parity sector, which is exemplified in Fig. 3. Therefrom, for a given filling fraction $\rho = N/L$ we can extract the scaling of two critical parameters separating the low-lying odd-parity cluster (blue in Fig. 3), which hosts the BEC ground state, from the remaining eigenstates. In what follows we set $t \equiv 1$ as unit of energy. The first critical hopping $\tilde{s}_{c,1}$ and gap Δ_1 arise once the clustered odd-parity eigenstates constitute the overall ground state, indicating the condensation of bosons into the k_0 mode
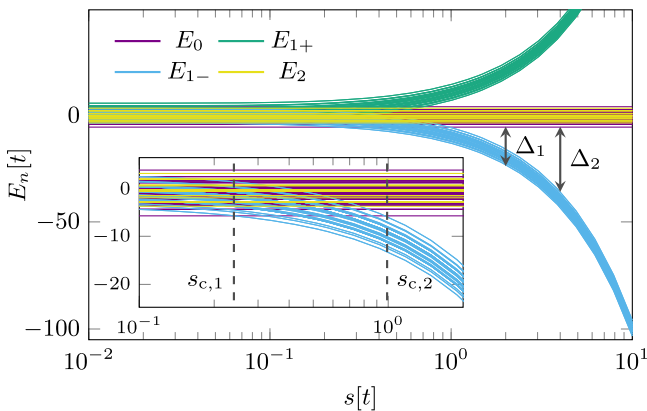

Fig. 3 Clustering of the many-particle eigenstates for a wheel composed of 10 lattice sites in the $N = 4$ particle number sector as a function of the ring-to-center hopping s. Different colors correspond to the eigenenergies $E_0, E_{1,\pm}, E_2$ of $\hat{H}_{\text{lad}}$ in the k_0-subspace Eq. (9), generating a clustering in the many-body spectrum. For each energy, we show all possible $k \neq k_0$ Slater determinants. Indicated are also the gaps defining the two critical ring-to-center hoppings, $s_{c,1}$ and $s_{c,2}$, describing the starting and complete separation of even and odd parity sectors, respectively.

(abbreviating $X_\rho = \frac{\sin(\pi\rho)}{\pi}$):

$$
\tilde{s}_{c,1} = \sqrt{8X_\rho}, \quad (11)
$$

$$
\Delta_1 = -\left(1 + 2X_\rho\right) + \sqrt{\left(1 - 2X_\rho\right)^2 + \tilde{s}^2}. \quad (12)
$$

The second critical hopping is defined by the complete separation of the odd-parity cluster from the even-parity many-particle eigenstates:

$$
\tilde{s}_{c,2} = 4L\sqrt{X_\rho^2 + \mathcal{O}(L^{-1})}, \quad (13)
$$

$$
\Delta_2 = -4LX_\rho - \left(1 - 2X_\rho\right) + \sqrt{\left(1 + 2X_\rho\right)^2 + \tilde{s}^2}. \quad (14)
$$

Note that $\tilde{s} > \tilde{s}_{c,2}$ implies that scattering between states with even and odd k_0 parity, caused by external perturbations, can only occur if the energy barrier Δ_2 can be overcome.

Discussion
The analytical solution and, in particular, the property of BEC ground states exhibiting odd $k = k_0$ parity allows to draw some striking conclusions on the stability of the BEC in the presence of local perturbations on the outer ring. Adding interactions acting on a finite subset of outer ring sites only, we note that in general the single-particle description breaks down in favor of a more complicated many-body state. Therefore, interactions generically couple the two parity sectors in the k_0 subspace and one might expect a breaking of the $\mathbb{Z}_2$-symmetry. However, mixing of the k_0 parity sectors caused by local interactions connecting d neighboring sites on the outer ring is of the order of $\sim \frac{Vd}{\tilde{s}}$ where V is the largest interaction strength. The consequence is that increasing the number of lattice sites, i.e. the center site's coordination number, the $\mathbb{Z}_2$ symmetry of the k_0 modes is approximately restored, thus stabilizing BEC in the presence of interactions on the outer ring.

We numerically checked the robustness of the BEC in the thermodynamic limit for $k_0 = 0$ and finite values of the ring-to-center hopping. To this end, we calculated the ground-state occupation $n_{k_0}(s, L)$ of the $k_0 = 0$ mode[1,38] using DMRG. Normalizing with respect to the upper bound on the condensate occupation $n_{\text{max}}(L) = L\rho(1 - \rho + 1/L)$[11], we extrapolated the condensate fraction into the thermodynamic limit $n_{k_0}(s)/n_{\text{max}} = \lim_{L\to\infty} \frac{n_{k_0}(s,L)}{n_{\text{max}}(L)}$, see Supplementary Note 5. The resulting extrapolations are shown in Fig. 4a for interaction strengths between $V = 0$ and $V = 1$ and particle densities between $\rho = 1/16$ and $1/2$. Note that even though there is a renormalization of the overall condensate fraction, we always observe a finite condensate density in the thermodynamic limit, even for strong interactions and high particle densities. To further demonstrate the asymptotic robustness of the $\mathbb{Z}_2$-symmetry protection, in Fig. 4b the dependency of the condensate fraction at finite system sizes and as a function of $V/\tilde{s}$ is shown. We also observe the behavior expected from our previous analysis, namely that the condensate occupation dominantly depends on the system size and the ratio between the interaction and the extensively scaling renormalized ring-to-center hopping $\tilde{s} = s\sqrt{L}$. In accordance to the scaling of Δ_2, the maximally possible condensation is reached if $\tilde{s} \sim L$. We emphasize that these relations can be translated to experimental realizations to determine the necessary coordination number, i.e. number of sites on the ring, to detect BEC in the presence of interactions.
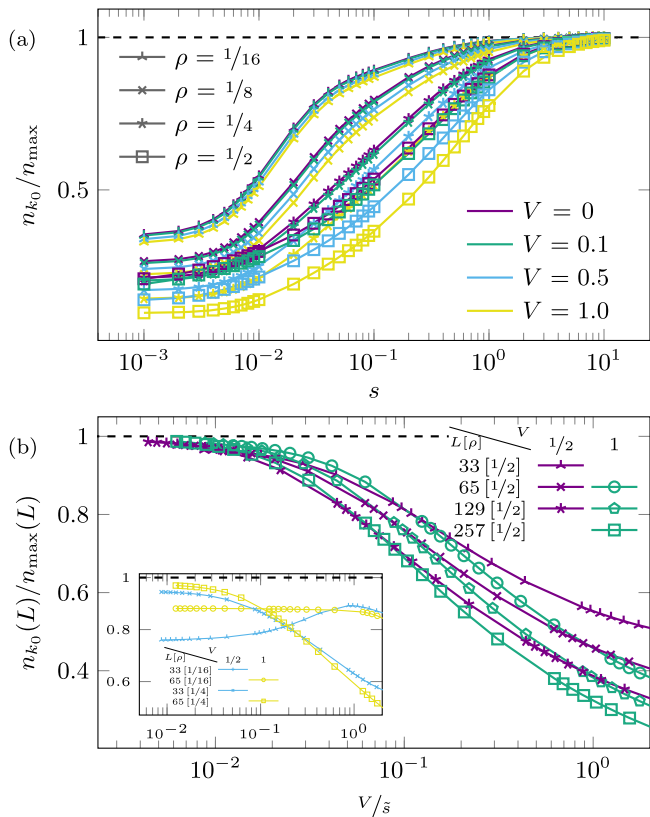
Fig. 4 Numerical analysis of the robustness of the Bose-Einstein condensate (BEC). a Ground-state condensate fraction n_{k_0} normalized to the maximally possible value n_{max}[11] and extrapolated to the thermodynamic limit. **b** Asymptotically the normalized condensate fraction for a fixed number of lattice sites L is a function of the ratio of nearest-neighbor interaction strength and rescaled hopping amplitude $V/\tilde{s}$, only. Results are shown for different V and densities on the ring ρ. Note that for very small fillings $\rho = 1/16$ (inset), there are significant deviations of the observed connection between the condensate fraction and the ratio $V/\tilde{s}$. This originates from the flat single-particle dispersion around $k = \pi$ (see Fig. 1). Thereby, the complete separation of the odd-parity states (controlled by the energy gap Δ_2) occurs already for small ring-to-center hoppings, mainly independent on the number of lattice sites.

Conclusion

Our findings imply important consequences for both experimental and theoretical realizations of wheel geometries in general. First of all, a particular single-particle mode can be gapped out by a proper modulation of the ring-to-center hopping, allowing the general protection of ordered phases that are characterized by a certain wave vector. We believe that such a modulation of the ring-to-center hopping provides an experimentally feasible approach to realize exotic, finite-momentum BEC in the framework of ultracold or Rydberg atoms[30–33,39–41]. Second, there is a many-body gap separating the BEC-carrying states from the remaining spectrum $\sim s\sqrt{L}$, i.e. large gaps can be realized by increasing the coordination number of the center site. The resulting robustness against interactions on the ring can be exploited to increase critical temperatures for phase transitions into otherwise highly fragile quantum phases. Possible applications are mesoscopic setups where a conducting center site may be contacted to one-dimensional ring geometries via tunnel contacts, allowing the stabilization of ordered states on the ring against perturbations. Such a scaling could also be exploited to achieve exceptionally stable logical qubits by coupling a set of noisy qubits to a central qubit. Experimental platforms providing
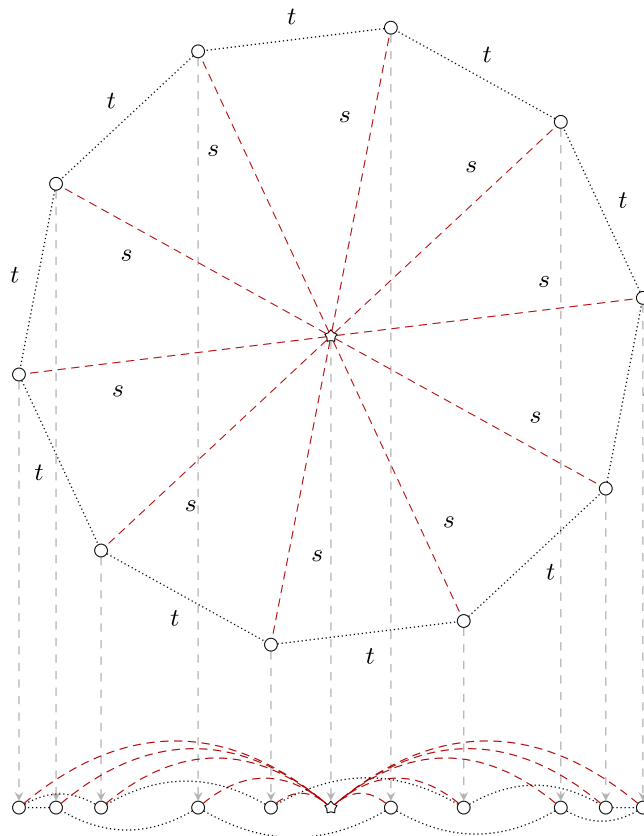

Fig. 5 Chosen projection of the wheel geometry (top) onto a chain (bottom). This reduces the long-range interaction from the first to the last site that is replaced by multiple NNN interactions compared to a straight forward periodic boundary implementation. The center site (star) of the wheel is placed in the middle of this chain—again in order to reduce the long-range interaction to a minimum.

the required all-to-one couplings are for example NV centers[42,43] or superconducting qubits in circuit QED settings[44]. Moreover, we believe that the wheel-to-ladder mapping could prove useful in the analysis of hidden fermions[45]. Further interesting questions are the incorporation of disorder on both the ring and center site, as well as the effect of (artificial) gauge fields and a rescaled ring-to-center hopping $s \to \frac{s}{\sqrt{L}}$ with regard to the crossover from one to an infinite number of dimensions.

Methods

Wheel-to-ladder mapping. One of our methodical key findings is a mapping that allows to utilize a JWT to construct the solution to the many-body problem. Closed analytic expressions for models exhibiting a true BEC are rare, in particular for the case of HCBs, which can be obtained, for instance, in the Bose-Hubbard model in the limit of infinitely strong on-site repulsion. We therefore elaborate on the mapping in more detail.

To solve the many-particle problem of the wheel Hamiltonian $\hat{H}$, we introduce a mapping between the long-range coupled wheel Hamiltonian and the NNN coupled ladder Hamiltonian $\hat{H}_{lad}$ with periodic boundary conditions depicted in Fig. 1. Since they exhibit the same matrix elements, we identify the subspace of the center site with the single-particle momentum states $|k = 0, N_\odot = 0, 1\rangle_\odot$ in the inner ring of the ladder, where $N_\odot$ is the occupation of the inner ring of the periodic ladder. Utilizing the projector to this subspace $\hat{\Pi}_\odot$, we can relate both Hamiltonians:

$$\hat{H} = \hat{\Pi}_\odot \hat{H}_{lad} \hat{\Pi}_\odot. \tag{15}$$

A JWT allows to express the hardcore bosonic ladder operators in terms of fermionic ones

$$\hat{c}_j^{(\dagger)} = \prod_{k<j} e^{i\pi\hat{n}_k} \hat{h}_j^{(\dagger)}, \text{ with } j = 0, \dots, 2L-1. \tag{16}$$

When transforming the hardcore bosonic Hamiltonian, the JWT leads to cancellations of arbitrarily long-ranged interactions and only a single phase-factor $e^{i\pi\hat{n}_{\odot j}}$ remains in the hopping terms on the outer ring $\hat{\Pi}_{\odot}\hat{h}_j^{\dagger}\hat{h}_{j+1}\hat{\Pi}_{\odot} = \hat{\Pi}_{\odot}\hat{c}_j^{\dagger}e^{i\pi\hat{n}_{\odot j}}\hat{c}_{j+1}^{\dagger}\hat{\Pi}_{\odot}$. At this point, the projected ladder Hamiltonian can be solved analytically.

Numerical methods. All numerical results were obtained using DMRG in its matrix-product state representation[27] implemented in the SYMMPS toolkit[46]. More precisely, the calculations were performed with a bond dimension up to 1200, which allowed the discarded weight to always stay below $2 \cdot 10^{-8}$ and usually below 10^{-10}. Since DMRG works best in one-dimensional systems, the wheel is projected onto a chain in a way that reduces the long-range interaction to a (rather large) minimum, see Fig. 5.

Observables. The observable of interest, as shown in Fig. 4, is the normalized condensate fraction of the distinguished k_0 mode extrapolated to the thermodynamic limit. Note that in our calculations we chose $k_0 = 0$. In order to obtain this quantity, we need to get the SPDM of the ground state,

$$\rho_{j,j'} = \langle \hat{c}_j^{\dagger} \hat{c}_{j'} \rangle \tag{17}$$

for multiple system sizes. The condensate fraction is then obtained by Fourier transforming the SPDM:

$$n_k = \frac{1}{L}\sum_{j,j'} e^{-2ik(j-j')/L} \rho_{j,j'}. \tag{18}$$

In order to be able to compare the condensate fractions for different system sizes, it is necessary to normalize them w.r.t. the maximally possible value. This is given by[11]

$$n_{\max}(L) = (L - N + 1) \cdot N/L. \tag{19}$$

We chose four different sizes of the outer ring (32, 64, 128, 256) and extrapolated these normalized results via a $1/L$ fit.

Data availability
The data that support the findings of the current study are available from the authors upon reasonable request.

Code availability
The software package SYMMPS[46] is available via www.symmps.eu. The source code is available from the authors upon reasonable request.

References
1. Penrose, O. & Onsager, L. Bose-einstein condensation and liquid helium. *Phys. Rev.* **104**, 576–584 (1956).
2. Anderson, M. H., Ensher, J. R., Matthews, M. R., Wieman, C. E. & Cornell, E. A. Observation of bose-einstein condensation in a dilute atomic vapor. *Science* **269**, 198–201 (1995).
3. Jaksch, D., Bruder, C., Cirac, J. I., Gardiner, C. W. & Zoller, P. Cold bosonic atoms in optical lattices. *Phys. Rev. Lett.* **81**, 3108–3111 (1998).
4. Bloch, I., Dalibard, J. & Zwerger, W. Many-body physics with ultracold gases. *Rev. Mod. Phys.* **80**, 885–964 (2008).
5. Dalfovo, F., Giorgini, S., Pitaevskii, L. P. & Stringari, S. Theory of bose-einstein condensation in trapped gases. *Rev. Mod. Phys.* **71**, 463–512 (1999).
6. Giamarchi, T., Rüegg, C. & Tchernyshyov, O. Bose-einstein condensation in magnetic insulators. *Nat. Phys.* **4**, 198 – 204 (2008).
7. de Escobar, Y. N. M. et al. Bose-einstein condensation of sr84. *Phys. Rev. Lett.* **103**, 200402 (2009).
8. Kraft, S., Vogt, F., Appel, O., Riehle, F. & Sterr, U. Bose-einstein condensation of alkaline earth atoms: Ca40. *Phys. Rev. Lett.* **103**, 130401 (2009).
9. van Dongen, P. G. J., Vergés, J. A. & Vollhardt, D. The hubbard star. *Zeitschrift für Physik B Condensed Matter* **84**, 383–392 (1991).
10. Vidal, E. J. G. G., Lima, R. P. A. & Lyra, M. L. Bose-einstein condensation in the infinitely ramified star and wheel graphs. *Phys. Rev. E* **83**, 061137 (2011).
11. Tennie, F., Vedral, V. & Schilling, C. Universal upper bounds on the bose-einstein condensate and the hubbard star. *Phys. Rev. B* **96**, 064502 (2017).
12. Máté, M., Legeza, Ö., Schilling, R., Yousif, M. & Schilling, C. How creating one additional well can generate bose-einstein condensation. *Communications Physics* **4**, 29 (2021).
13. Wilson, K. G. The renormalization group: Critical phenomena and the kondo problem. *Rev. Mod. Phys.* **47**, 773 (1975).
14. Georges, A., Kotliar, G., Krauth, W. & Rozenberg, M. J. Dynamical mean-field theory of strongly correlated fermion systems and the limit of infinite dimensions. *Rev. Mod. Phys.* **68**, 13 (1996).
15. Freericks, J. K., Turkowski, V. M. & Zlatić, V. Nonequilibrium dynamical mean-field theory. *Phys. Rev. Lett.* **97**, 266408 (2006).
16. Eckstein, M. & Werner, P. Nonequilibrium dynamical mean-field simulation of inhomogeneous systems. *Phys. Rev. B* **88**, 075135 (2013).
17. Aoki, H. et al. Nonequilibrium dynamical mean-field theory and its applications. *Rev. Mod. Phys.* **86**, 779–837 (2014).
18. Seth, P., Krivenko, I., Ferrero, M. & Parcollet, O. Triqs/cthyb: A continuous-time quantum monte carlo hybridisation expansion solver for quantum impurity problems. *Computer Physics Communications* **200**, 274–284 (2016).
19. Gaudin, M. Diagonalisation d'une classe d'hamiltoniens de spin. *J. Phys. France* **37**, 1087–1098 (1976).
20. Prokof, N. V. & Stamp, P. C. E. Theory of the spin bath. *Rep. Prog. Phys.* **63**, 669–726 (2000).
21. von Delft, J. & Ralph, D. Spectroscopy of discrete energy levels in ultrasmall metallic grains. *Phys. Rep.* **345**, 61–173 (2001).
22. Taylor, J. M., Imamoglu, A. & Lukin, M. D. Controlling a mesoscopic spin environment by quantum bit manipulation. *Phys. Rev. Lett.* **91**, 246802 (2003).
23. Dukelsky, J., Pittel, S. & Sierra, G. Colloquium: Exactly solvable richardson-gaudin models for many-body quantum systems. *Rev. Mod. Phys.* **76**, 643–662 (2004).
24. Villazon, T., Chandran, A. & Claeys, P. W. Integrability and dark states in an anisotropic central spin model. *Phys. Rev. Res.* **2** https://doi.org/10.1103/PhysRevResearch.2.032052 (2020).
25. Ashida, Y. et al. Quantum rydberg central spin model. *Phys. Rev. Lett.* **123**, 183001 (2019).
26. Schollwöck, U. The density-matrix renormalization group. *Rev. Mod. Phys.* **77**, 259 (2005).
27. Schollwöck, U. The density-matrix renormalization group in the age of matrix product states. *Annals Phys.* **326**, 96 – 192 (2011). January 2011 Special Issue.
28. White, S. R. Density matrix formulation for quantum renormalization groups. *Phys. Rev. Lett.* **69**, 2863–2866 (1992).
29. White, S. R. Density-matrix algorithms for quantum renormalization groups. *Phys. Rev. B* **48**, 10345–10356 (1993).
30. Lim, L.-K., Smith, C. M. & Hemmerich, A. Staggered-vortex superfluid of ultracold bosons in an optical lattice. *Phys. Rev. Lett.* **100**, 130402 (2008).
31. Hick, J., Sauli, F., Kreisel, A. & Kopietz, P. Bose-einstein condensation at finite momentum and magnon condensation in thin film ferromagnets. *Eur. Phys. J. B* **78**, 429–437 (2010).
32. Di Liberto, M., Tieleman, O., Branchina, V. & Smith, C. M. Finite-momentum bose-einstein condensates in shaken two-dimensional square optical lattices. *Phys. Rev. A* **84**, 013607 (2011).
33. Lin, Y.-J., Jiménez-García, K. & Spielman, I. B. Spin–orbit-coupled bose–einstein condensates. *Nature* **471**, 83–86 (2011).
34. Rigol, M. & Muramatsu, A. Ground-state properties of hard-core bosons confined on one-dimensional optical lattices. *Phys. Rev. A* **72**, 013604 (2005).
35. Rigol, M. & Muramatsu, A. Emergence of quasicondensates of hard-core bosons at finite momentum. *Phys. Rev. Lett.* **93**, 230404 (2004).
36. Lieb, E. H. & Liniger, W. Exact analysis of an interacting bose gas. i. the general solution and the ground state. *Phys. Rev.* **130**, 1605–1616 (1963).
37. Lieb, E. H. Exact analysis of an interacting bose gas. ii. the excitation spectrum. *Phys. Rev.* **130**, 1616–1624 (1963).
38. Yang, C. N. Concept of off-diagonal long-range order and the quantum phases of liquid he and of superconductors. *Rev. Mod. Phys.* **34**, 694–704 (1962).
39. Summy, G. & Wimberger, S. Quantum random walk of a bose-einstein condensate in momentum space. *Phys. Rev. A* **93**, 023638 (2016).
40. Mangaonkar, J. et al. Effects of finite momentum width on the reversal dynamics in a BEC based atom optics-kicked rotor. *Journal of Physics B: Atomic, Molecular and Optical Physics* **53**, 235502 (2020).
41. Eiles, M. T., Eisfeld, A. & Rost, J. M. Anderson localization of a rydberg electron. *arXiv* https://arxiv.org/pdf/2111.10345.pdf (2021).
42. Goldman, M. L. et al. State-selective intersystem crossing in nitrogen-vacancy centers. *Phys. Rev. B* **91**, 165201 (2015).
43. Pezzagna, S. & Meijer, J. Quantum computer based on color centers in diamond. *Appl. Phys. Rev.* **8**, 011308 (2021).
44. Krantz, P. et al. A quantum engineer's guide to superconducting qubits. *Appl. Phys. Rev.* **6**, 021318 (2019).
45. Sakai, S., Civelli, M. & Imada, M. Hidden fermionic excitation boosting high-temperature superconductivity in cuprates. *Phys. Rev. Lett.* **116**, 057003 (2016).

46. Paeckel, S. & Köhler, T. SymMPS. https://www.symmps.eu. Accessed: 2021-04-01.

Author contributions

S.P., T.K. and R.H.W. developed the idea of the wheel-to-ladder mapping. S.P., R.H.W. and F.A.P. worked out the theoretical analysis. T.K. performed all DMRG simulations. All authors contributed to the writing of the manuscript.

Competing interests

The authors declare no competing interests.

Additional information

Supplementary information The online version contains supplementary material available at https://doi.org/10.1038/s42005-023-01303-z.

Correspondence and requests for materials should be addressed to Reja H. Wilke.

Peer review information : *Communications Physics* thanks the anonymous reviewers for their contribution to the peer review of this work.

Reprints and permission information is available at http://www.nature.com/reprints

Publisher's note Springer Nature remains neutral with regard to jurisdictional claims in published maps and institutional affiliations.